Mathematical Biosciences 377 (2024) 109292

Contents lists available at ScienceDirect

Mathematical Biosciences

journal homepage: www.elsevier.com/locate/mbs

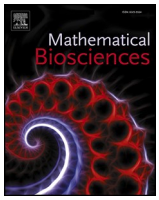

Original research article

Predicting the impact of retinal vessel density on retinal vessel and tissue oxygenation using a theoretical model

Brendan C. Fry [a], Croix Gyurek [b], Amanda Albright [b], George Eckert [c], Janet Coleman-Belin [d], Alice Verticchio [d], Brent Siesky [d], Alon Harris [d,1], Julia Arciero [b,1,*]

[a] Department of Mathematics and Statistics, Metropolitan State University of Denver, P.O. Box 173362, Campus Box 38, Denver, CO 80217, USA
[b] Department of Mathematical Sciences, Indiana University Indianapolis, 402 N. Blackford St, LD 270, Indianapolis, IN 46202, USA
[c] Department of Biostatistics and Health Data Science, Indiana University School of Medicine and Richard M. Fairbanks School of Public Health, 410 W. 10th St, Indianapolis, IN 46202, USA
[d] Department of Ophthalmology, Icahn School of Medicine at Mount Sinai Hospital, One Gustave L. Levy Place, Box 1183, New York, NY 10029, USA

ARTICLE INFO

Keywords:
Vessel density
Mathematical model
Retina
Glaucoma
Oxygenation
Blood flow

ABSTRACT

Vascular impairments, including compromised flow regulation, have been identified as significant contributors to glaucomatous disease. Recent studies have shown glaucoma patients with significantly reduced peripapillary, macular, and optic nerve head vessel densities occurring with early glaucomatous structural changes prior to detectable visual field loss. This study aims to quantify the potential impact of decreased vessel densities on retinal perfusion and oxygen metabolism. In our clinical observations, pre-perimetric glaucoma patients exhibited a 10–13 % reduction in vessel density compared to healthy individuals. Our theoretical model of the retinal vasculature is adapted in this study to assess the potential impact of this reduction in vessel density on retinal oxygenation. The model predicts a 1 % and 38 % decrease in mean oxygen saturation in retinal vessels immediately downstream of the capillaries when vessel density is decreased from its reference value by 10 % and 50 %, respectively. The impact of capillary loss on oxygen extraction fraction and the partial pressure of oxygen in retinal tissue is also predicted. Reductions in vessel density are simulated in combination with impaired flow regulation, and the resulting effects on saturation and flow are predicted. The model results showed a nonlinear relationship between vessel density and downstream saturation, indicating that larger decreases in the density of capillaries have a disproportionate impact on oxygenation. The model further demonstrates that the detrimental effects of minor vessel density reductions are exacerbated when combined with other vascular impairments.

1. Introduction

Open angle glaucoma (OAG) is the second leading cause of blindness worldwide and has a wide array of known and theorized contributing risk factors that lead to the destruction of retinal ganglion cells (RGC) and irreversible vision loss. While lowering intraocular pressure (IOP) is the only currently approved therapeutic target for OAG patients, impairments to oxygen delivery, tissue perfusion, and autoregulation have also been identified as significant contributors to glaucoma disease [1]. In addition, recent studies [2-9] have used optical coherence tomography angiography (OCTA) to reveal significant reductions in the vessel density (VD) of the peripapillary retina, optic nerve head (ONH), and macular regions in OAG patients compared to healthy controls.

Currently, data on early vascular changes are scarce in patients with pre-perimetric OAG, which is defined by the occurrence of characteristic structural glaucomatous changes in the ONH and retinal nerve fiber layer (RNFL) prior to significant visual field defects. Analysis in the earliest stages of glaucoma is vital to understand if vascular insult occurs

Abbreviations: DCP, Deep capillary plexus; ICP, Intermediate capillary plexus; IOP, Intraocular pressure; OAG, Open angle glaucoma; OCTA, Optical coherence tomography angiography; OEF, Oxygen extraction fraction; ONH, Optic nerve head; RGC, Retinal ganglion cell; RNFL, Retinal nerve fiber layer; RPC, Radial peripapillary capillary; SCP, Superficial capillary plexus; VD, Vessel density; VSM, Vascular smooth muscle; ANOVA, analysis of variance; C, Capillaries; PO2, Partial pressure of oxygen; LV, Large venules; SV, Small venules.

* Corresponding author at: 402 N. Blackford St., LD 270D, Indianapolis, IN 46202.
E-mail address: jarciero@iu.edu (J. Arciero).

[1] Contributed equally as senior authors.

https://doi.org/10.1016/j.mbs.2024.109292
Received 18 March 2024; Received in revised form 3 September 2024; Accepted 4 September 2024
Available online 5 September 2024

prior to and/or in conjunction with RGC loss. Although many studies have associated vascular insufficiency with glaucoma, the exact mechanisms of RGC death and sequence of changes observed in OAG remain poorly understood.

A recent prospective, cross-sectional study identified significantly reduced peripapillary, macular, and ONH VD in OAG patients in conjunction with early glaucomatous structural changes occurring prior to detectable visual field loss [10]. Such early capillary loss prior to functional loss may indicate a primary role for vascular dysfunction in OAG pathophysiology. It is therefore essential to gain a more complete understanding of the effects of capillary loss on retinal perfusion and oxygenation. In this study, theoretical modeling based on prospective clinical observations is used to predict how reductions in VD impact the blood flow and oxygenation of retinal tissue.

Previous mathematical modeling studies have addressed certain aspects involving the role of capillaries in microvascular blood flow distribution within various tissues. Fry et al. [11] used a theoretical model of blood flow regulation to demonstrate that observed capillary recruitment in response to changing metabolic conditions in hamster cremaster preparations can occur via the local control of arteriolar tone combined with nonuniform hematocrit partitioning at vessel bifurcations. However, this study did not examine the effects of varying vessel density. Goldman et al. [12] used modeling to show that the abnormal microvascular perfusion observed in skeletal muscle during sepsis could be described by varying the distribution of normal, fast, and stopped capillaries. They showed that decreased functional capillary density and increased oxygen consumption rate could lead to regions of severe hypoxia. However, this study did not allow for blood flow regulation (i.e., vessels could not dynamically change diameters in response to changing densities or oxygen consumption) and used a simplified non-heterogeneous description of the microvasculature, which can lead to underestimates of tissue hypoxia and partial pressure of oxygen (PO_2) spread [13]. Chiaravalli et al. [14] utilized a multi-scale/multi-physics mathematical model to quantify the impact of two hypothesized capillary configurations on retinal hemodynamics and oxygenation. The study compared model predictions when the superficial capillary plexus (SCP), intermediate capillary plexus (ICP), and deep capillary plexus (DCP) were connected in series or in parallel. Their model simulations showed larger pressure drops in the DCP and ICP than SCP when connected in series, and it showed that the blood flow redistributed uniformly when the three plexuses were connected in parallel. Capillary density values for each layer were obtained from Campbell et al. [15]. While providing helpful insight into oxygenation and hemodynamics, the model used in Chiaravalli et al. did not consider changes to vessel density values nor did it account for the heterogeneous vascular structure or flow regulation mechanisms within the human retina.

In this study, our previously developed theoretical model [16], which accounts for heterogeneous arteriolar network structure, flow regulation mechanisms, and oxygen transport, is used to assess the hemodynamic impact of clinically observed reductions in VD in patients with OAG. Although the original version of the model began as a mouse model, the model was scaled to represent a human retinal vascular network [17] and can be used in this study for comparisons to human data. Changes in IOP are not considered in this study by design so that the model simulations can isolate the vascular effects of vessel density changes. More specifically, the model is used to predict the partial pressure of oxygen (PO_2) and oxyhemoglobin saturation in retinal vessels and tissue for varied levels of VD, with an ultimate goal of complementing clinical studies to demonstrate possible consequences of capillary loss in glaucoma disease.

2. Materials and methods

2.1. Clinical measures

Our team recently published a study from which we obtained clinical VD data for use in the current modeling study [10]. Vessel densities of the ONH and macular regions were assessed using OCTA (Optovue Inc, Avanti Angiovue, Fremont, CA, USA), as depicted in Fig. 1. The principles and mechanisms behind OCTA calculations are complex [18-20] and involved consecutive scans, removal of artifacts using validated software algorithms, calculation of motion contrast to convert tissue reflectance into flow signals, and computation of VD as a percentage of assessed area [21]. A 4.5 mm HD Angio Disc scan was specifically used to assess the ONH VD (percentage of area occupied by OCTA detected vasculature) in the radial peripapillary capillary (RPC) slab (from the internal limiting membrane to the RNFL). ONH VDs were acquired within the optic disc region, the peripapillary region (identified by two concentric rings of 2.0 mm and 4.0 mm centered on the optic disc center), and the combination of these two regions. VDs were identified for all vessels (ALL) and small vessels (SV) using large-vessel masking (with threshold of $\geq$ 3 pixels, approximately $\geq$ 33 μm). The study included ONH VD assessments globally and peripapillary from the RPC slab (hemispheric for both ALL and SV) and regionally divided SV density parameters in all quadrants (superior, temporal, nasal, and inferior). Additionally, central macular VD was assessed using a 6.0 mm HD AngioRetina scan in the 1.0 mm central ring of the ETDRS grid radiating from the fovea [21]. Repeated measures ANOVA was used to evaluate differences in vessel density due to glaucoma status (glaucoma/healthy) and quadrant, adjusted for age, sex, and race. The ANOVA allowed different variances for the glaucoma and healthy groups, homogeneous variances for the four quadrants, and allowed correlations among sectors to vary. Pair-wise comparisons were adjusted for multiple comparisons using the Bonferroni method with a 5 % overall significance level. Analyses were performed using the gls function of the R statistical software package. Further details regarding the methods and initial differential results of OCTA data in patients with OAG and healthy controls may be found in [10].

2.2. Theoretical model of the retina

A published theoretical model of the human retina [16], which includes a combined heterogeneous representation of retinal arterioles and compartmental representation of capillaries, small venules, and large venules, is adapted in this study to isolate the potential impact of VD on retinal vessel and tissue oxygenation.

2.2.1. Geometry of the hybrid model

In this study, the theoretical model of a full retinal microvascular network is referred to as a "hybrid" model because it combines a heterogeneous spatial representation of the arteriolar network with a compartmental representation of the capillaries and venules [16]. The arteriolar network in the hybrid model was mapped from confocal microscopy images obtained from mice and adapted and scaled to human. Specifically, since a human retina has only four main arteriolar branches while a mouse retina has six, two branches from the mouse network were eliminated. The angles between the branches were adjusted based on human oximetry images. Finally, the diameters and lengths of the vessels were scaled by a factor of 3.6 and 5.9, respectively, based on human retinal measurements. This adaptation from mouse to human retina is also described in our previous work [17]. This network obtained originally from mouse is incredibly useful because it provides a physiologically accurate branching structure for this study. For computational ease, a single feed artery ("Branch 1″) is simulated in this

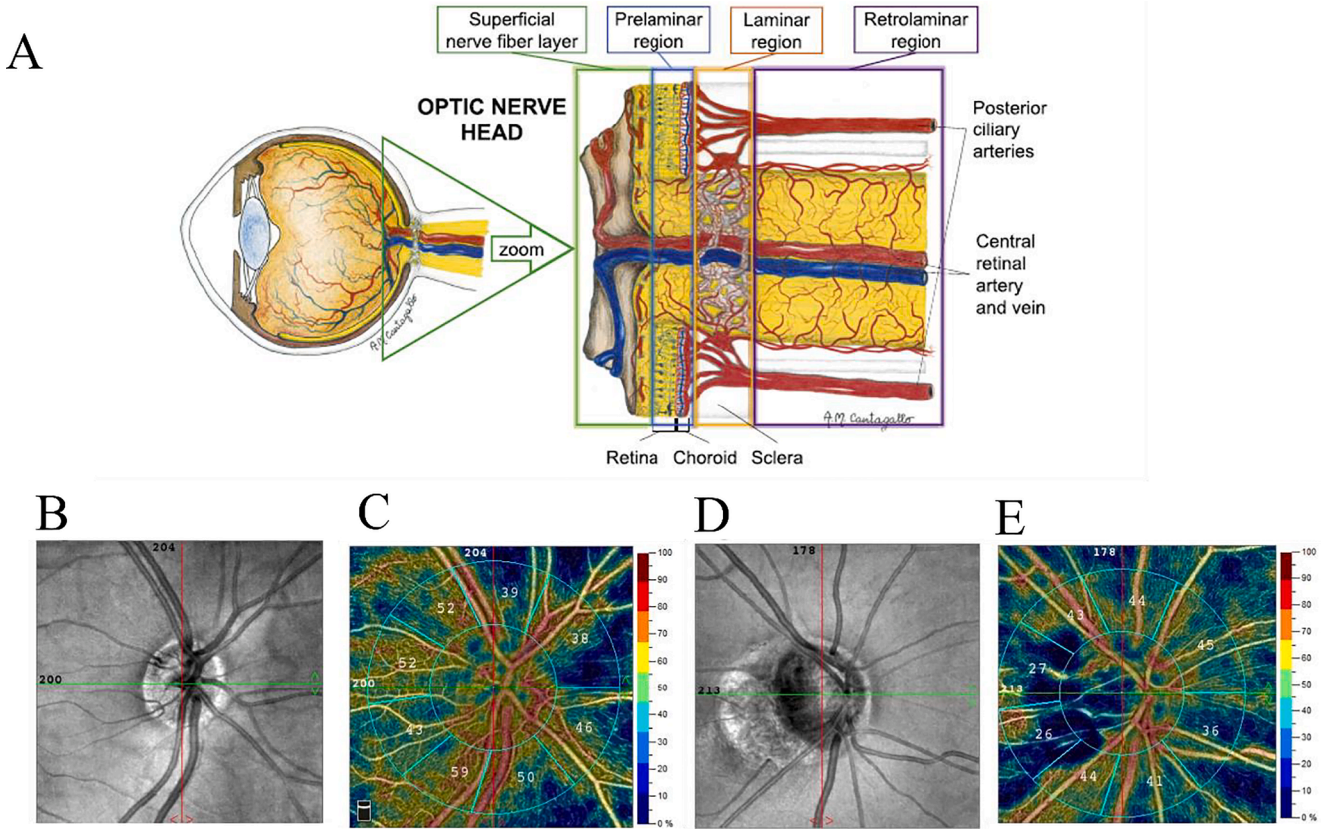

Fig. 1. A: Schematic representation of the anatomy and vascular supply of the optic nerve head (ONH) including the superficial nerve fiber layer, the prelaminar region, the laminar region, and the retrolaminar region [reproduced with permission from [22]. B-E: Images derived from optical coherence tomography angiography (OCTA) of a healthy subject (panels B and C) and an open-angle glaucoma patient (panels D and E). Panels B and D: Scanning laser ophthalmoscope-like image of the ONH region. Panels C and E: color-coded vessel density (VD) map in the radial peripapillary capillary (RPC) slab. The RTVue XR Avanti System (RTVue XR, Version 2018.1.1.63, Optovue Inc, Fremont, CA, USA) was used to assess VD as percentage of area occupied by OCTA-detected vasculature in the ONH region. ONH VD was measured in the 4.5 mm HD Angio Disc scan in the RPC slab (from the internal limiting membrane to the nerve fiber layer) in the entire region ("whole image"), and in the "peripapillary" region (defined by 2 rings of 2 mm and 4 mm centered on the disc center). The VD was measured for the small vessels (i.e., with large vessel masking) and for all vessels ("ALL"); the application of large vessel mask has a threshold of $\geq$3 pixels ($\sim \geq$ 33 μm) [23].

study, although the complete model contains all four feed arteries and 485 pathways. The number of pathways is not scaled between mouse and human, since branching structure is a physiological characteristic assumed to be consistent between species; only the vessel positions and magnitudes of vessel diameter and length are assumed to differ between mice and humans.

Compartments representing downstream capillaries (C), small venules (SV), and large venules (LV) are appended downstream of each of

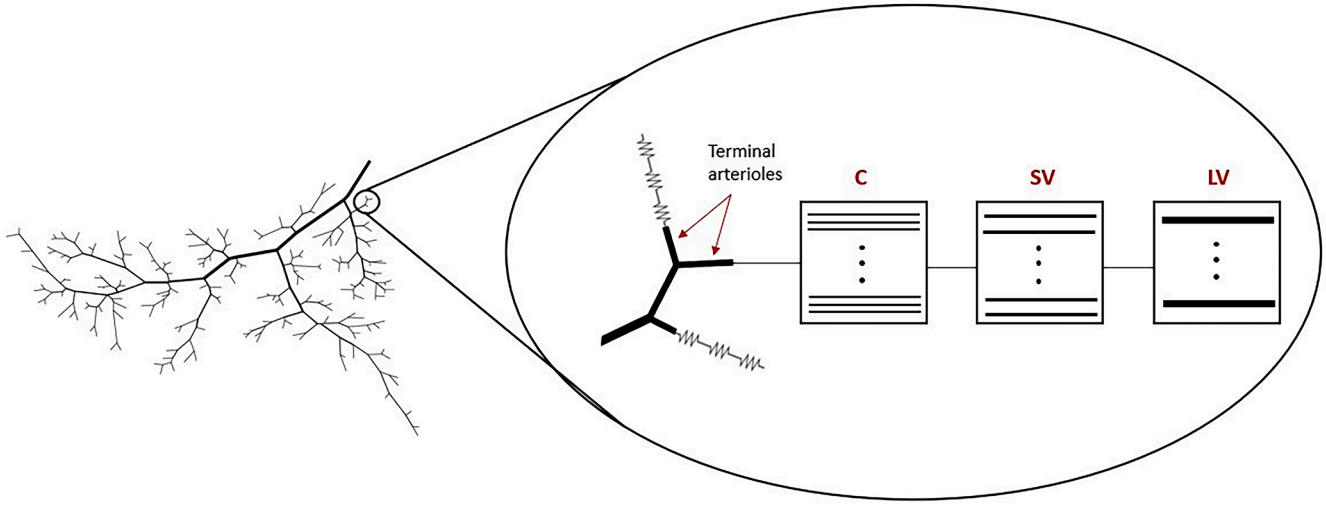

Fig. 2. Schematic of hybrid model. The arterioles are represented with spatial heterogeneity, and each terminal arteriole is connected to a series of compartments (resistors) representing downstream capillaries (C), small venules (SV), and large venules (LV), as shown in the enlargement. Reproduced with permission from [16].

the 171 terminal arterioles in Branch 1, as illustrated in Fig. 2. Each compartment consists of identical, parallel-arranged segments that are exposed to the same hemodynamic and metabolic conditions. Capillaries are assumed to have a fixed diameter of 6 μm, a fixed shear stress of 15 dyn/cm^2, and a fixed viscosity of 9.05 cP. These assumptions dictate flow through a single capillary. The number of capillaries in any compartment downstream of a terminal arteriole is determined via the conservation of flow, which requires that flow through the i'th terminal arteriole ($Q_{TA,i}$) is equal to the product of the number of capillaries ($n_{c,i}$) in the compartment and the flow through an individual capillary (Q_C). Given these calculations, an average of 412 capillaries comprises each compartment, with a maximum of 2627 capillaries and minimum of 9 capillaries depending on the pathway [16]. Fractional flows (and thus oxygen levels) enter each series of capillary and venous compartments downstream of the terminal arterioles, preserving heterogeneity of the network.

The numbers, diameters, and lengths of the small and large venules in each compartment are dictated by conservation of flow and loose symmetry assumptions. In particular, it was assumed that each terminal arteriole was associated with a corresponding small venule, and that the lengths of these corresponding compartments were the same. Similarly to the above capillary compartment description, conservation of flow dictated that the product of the number of small/large venules emanating from each terminal arteriole and the flow through each small/large venule must equal the flow through the given terminal arteriole. The treatment of the venous compartments is described in full detail in [17]. Table 1 provides the diameter, length, and vessel number for the capillary, small venule, and large venule compartments averaged over all 171 pathways.

2.2.2. Hemodynamics and flow regulation

As in [16], the microvascular network of the hybrid model is represented as a directed graph, where the vessels are the edges, and the vessel junctions are the nodes of the graph. It is assumed that pressure-driven flow through each vessel of the network is governed by Poiseuille's Law, $Q = \Delta P \frac{\pi D^4}{128 L \nu}$, where Q is the volumetric blood flow rate in the vessel, ΔP is the pressure drop along the vessel, D is the diameter of the vessel, L is the length of the vessel, and ν is the apparent viscosity of the blood in the vessel.

The pressure entering Branch 1 is assumed to be 40 mmHg (based on outgoing pressure measurements in the central retinal artery [24]), and the pressure at the downstream end of the venules in each pathway is assumed to be the value of IOP (taken here to be 15 mmHg). At each junction within the network, the principle of mass conservation was enforced, enabling the calculation of flow rate, hematocrit, and apparent viscosity in each arteriole through an iterative process [25]. A repository for the code used for this flow calculation method is provided at https://github.com/secomb/NetFlowV2. Subsequently, flows within the downstream capillary and venous compartments were calculated using Poiseuille's Law in conjunction with conservation of mass.

The model allows for the regulation of blood flow, whereby diameters of the arterioles change in response to changes in the activation level of surrounding vascular smooth muscle (VSM). A previously established theoretical model of blood flow regulation in the arterioles (described in detail in [26-29]) is used here to simulate changes in vascular tone in response to various stimuli. Namely, regulating arterioles are assumed to constrict and dilate due to the contraction and relaxation of the VSM, which is dictated by myogenic (pressure), shear-dependent (flow), and metabolic (oxygen) responses. Briefly, the vessel wall mechanics are assumed to be governed by the Law of Laplace (Eq. (1)) whereby the circumferential wall tension, T, balances the pressure difference across the vessel wall to maintain the diameter of the vessel:

$$T = \frac{(P - P_I)D}{2} \tag{1}$$

where P_I is the intraocular pressure, and P is the intraluminal blood pressure. The total tension ($T_{total} = T_{pass} + AT_{act}^{max}$) in the vessel wall is assumed to be the combination of passive tension ($T_{pass} = C_{pass} e^{C'_{pass}\left(\frac{D}{D_0} - 1\right)}$), which results from structure components of the vessel wall and is given by an exponential function of vessel diameter based on measured nonlinear increases in tension with circumferential length [30], and active tension (AT_{act}^{max}), which results from activation of vascular smooth muscle in the vessel wall, where A is the level of smooth muscle activation in a given vessel ranging between 0 and 1, and $T_{act}^{max} = C_{act} e^{-\left(\frac{\frac{D}{D_0} - C'_{act}}{C''_{act}}\right)^2}$ is a Gaussian function of vessel diameter. D_0 represents the passive diameter (i.e., $A = 0$) of the vessel at a pressure of 40 mmHg. The level of smooth muscle activation (A_{total}, Eq. (2)) for a given vessel is modeled as a sigmoidal function of the input stimulus (denoted S_{tone}, Eq. (3)) which is assumed to be a function of the myogenic response, the shear-dependent response, and the metabolic response:

$$A_{total} = \frac{1}{1 + \exp(-S_{tone})} \tag{2}$$

$$S_{tone} = C_{myo} T_{total}(D) - C_{shear} \tau_{wall}(D, Q) - C_{meta} S_{meta}(P_{O2}) + C'_{tone} \tag{3}$$

Increases in activation lead to vessel constriction (i.e., positive terms in Eq. (3) for the myogenic response), and decreases in activation lead to vessel dilation (i.e., negative terms in Eq. (3) for the shear response and conducted metabolic response). From an assumed initial control (reference) state, changes in vessel diameter and activation are assumed to be governed by the following set of differential equations in each arteriole:

$$\frac{dD}{dt} = \frac{1}{\tau_d} \frac{D_c}{T_c} (T - T_{total}(D, A)) \tag{4}$$

$$\frac{dA}{dt} = \frac{1}{\tau_a} (A_{total}(D, A) - A) \tag{5}$$

where τ_d and τ_a are time constants for diameter and activation, respectively, and D_c and T_c are the control (reference) state diameter and tension, respectively. Parameter values for this model have been estimated and validated in previous modeling studies [11,17,26,28,29,31-33] and are given in Table 2.

2.2.3. Oxygen transport

Oxygen transport in the arteriolar tissue is governed by the steady-state diffusion equation with consumption, assumed here to have a Michaelis-Menten saturating form:

$$D_{diff} \alpha \nabla^2 P_{O2}(x, y, z) = M_0 \frac{P_{O2}(x, y, z)}{P_0 + P_{O2}(x, y, z)} \tag{6}$$

where D_{diff} and α are the diffusivity and solubility of oxygen in the arteriolar tissue, respectively, P_{O2} is the tissue partial pressure of oxygen at tissue point (x,y,z), M_0 is the maximum oxygen consumption rate in tissue (herein referred to as oxygen demand), and P_0 is the PO_2 at which

Table 1
Diameter, number, and length of segments in capillary, small venule, and large venule compartments averaged over all pathways.

Description	C	SV	LV
Diameter, D (μm)	6	31.3	159
Number of segments, n	412	1	0.006
Length, L (cm)	0.080	0.032	0.938

Table 2
Parameter values for vessel wall mechanics (flow regulation) model.

Description	Parameter	Value	Unit	Reference
VSM activation sensitivity	C_{myo}	$1.37/D_0$	cm/dyn	[11]
VSM shear stress sensitivity	C_{shear}	0.0258	cm^2/dyn	[28]
VSM metabolic sensitivity	C_{meta}	1000	1/μM/cm	[29]
VSM constant	C'_{tone}	52–205		Calculated
Passive tension strength	C_{pass}	$1.67 \cdot D_0$	dyn/cm	calculated
Passive tension sensitivity	C'_{pass}	$-0.027 \cdot D_0 + 12.52$		[26]
Max active peak tension	C_{act}	$1.30 \cdot D_0^{1.48}$	dyn/cm	[11]
Max active length dependence	C'_{act}	$-0.00146 \cdot D_0 + 1.13$		[28]
Max active tension range	C''_{act}	$-0.00146 \cdot D_0 + 0.308$		[28]
Passive reference diameter	D_0	29–151	μm	calculated
Time constant for diameter	τ_d	1	s	[26]
Time constant for activation	τ_a	20	s	[11]
Control state diameter	D_c	22–117	μm	[17]
Control state tension	T_c	13–188	dyn/cm	[17]
Vessel length	L	38–2224	μm	[17]

Table 3
Parameter values for oxygen transport model.

Description	Parameter	Value	Unit	Reference
Krogh diffusion coefficient	$D_{diff}\alpha$	6×10^{-10}	cm^3 O_2/cm/s/mmHg	[31,32]
Oxygen demand	M_0	1 - 4	cm^3 O_2/100 cm^3/min	varied
Michaelis Menten constant for O_2 consumption	P_0	10	mmHg	[33]
Tissue width of Krogh Cylinder	d	20–36	μm	calculated

the consumption rate is half maximal (i.e., Michaelis Menten half saturation constant). All parameter values are listed in Table 3.

In the arteriolar network, which is comprised of a spatially heterogeneous distribution of vessels, a Green's function method was used to solve Eq. (6), whereby the arterioles were represented as oxygen sources and the tissue points as oxygen sinks [34,35]. The oxygen level at a given tissue point was then computed as the superposition of the oxygen fields (i.e., the Green's functions) resulting from each of the vessel oxygen sources. This method allows for the efficient computation of oxygen levels in a heterogeneous network and accounts for the diffusive interactions among all tissue points and vessels throughout the network. A repository for the Green's function method is provided at https://github.com/secomb/GreensV4_GPU.

By conservation of mass, in each vessel segment,

$$\frac{df(P_b)}{ds} = -q_v(s) \tag{7}$$

where $f(P_b) = Q(H_D C_0 S(P_b) + \alpha_b P_b)$ is the convective O_2 transport rate, H_D is the discharge hematocrit, C_0 is the hemoglobin-bound O_2 concentration in a fully saturated red blood cell, P_b is the blood PO_2, α_b is the solubility of O_2 in blood, s is the length along the vessel segment, $q_v(s)$ is the rate of diffusive O_2 efflux per unit length, and $S(P_b)$ is the oxyhemoglobin saturation, given as a function of blood PO_2 by a Hill equation:

$$S(P_b) = \frac{P_b^n}{P_b^n + P_{50}^n} \tag{8}$$

with $P_{50} = 26$ mmHg and $n = 2.7$ [36].

In the downstream venous and capillary compartments, similarly to Eq. (7), conservation of mass gives the following rate of change of O_2 flux:

$$\frac{d\left(Q_j H_D C_0 S(P_b(s))\right)}{ds} = -q_v(s) \tag{9}$$

where j indicates the index of a given compartment, and s is the length along the compartment.

In the downstream capillary compartments, oxygen transport was simulated using a Krogh cylinder model [26,27,37,38], whereby vessels are arranged in parallel, with each cylindrical vessel surrounded by a sleeve of tissue into which oxygen diffuses (see Fig. 3). The governing equation for this process is the steady-state radial diffusion equation with a consumption term:

$$D_{diff}\alpha\left[\frac{1}{r}\frac{d}{dr}\left(r\frac{dP_{O2}(s,r)}{dr}\right)\right] = M_0 \tag{10}$$

where r is the radial distance within the tissue cylinder, s is the length along the capillary segment, and M_0 is the maximum oxygen consumption rate (assumed constant) in the capillaries. The Krogh cylinder model assumes that the PO_2 of the blood is equal to the PO_2 at the blood-tissue interface (i.e., $P_{O2}(s, r_c) = P_b(s)$) and that there is no flux at the tissue boundary (i.e., $\frac{dP_{O2}(s,r_t)}{dr} = 0$). The capillary is discretized into 100 segments along its length. At each point along the capillary, Eq. (9) is solved to obtain the PO_2 of the blood ($P_b(s)$), and then the PO_2 in the radial direction of the tissue cylinder ($P_{O2}(s,r)$) is obtained by solving Eq. (10) analytically. Oxygen extraction is negligible in venules and is thus neglected in this model.

The O_2 consumption rate per vessel length (i.e., q_v in Eq. (9)) in the downstream capillary tissue was computed as:

$$q_v = \int_{r_c}^{r_t} M_0 2\pi r \, dr = M_0 \pi\left(r_t^2 - r_c^2\right) \tag{11}$$

where r_c is the radius of the capillary, and r_t is the radius of surrounding tissue. The tissue width that surrounds each capillary is defined to be $d = r_t - r_c$, and is dependent on the vessel density, VD. As in [17], the vessel density is defined as

$$VD = \frac{\sum_i n_{C,i} L_{C,i}}{\underbrace{VOL_A}_{\substack{\text{Arteriolar} \\ \text{contribution}}} + \sum_i \underbrace{\left[n_{C,i} L_{C,i} \pi \left(r_{C,i} + d\right)^2\right]}_{\substack{\text{Capillary} \\ \text{contribution}}} + \underbrace{n_{SV,i} L_{SV,i} \pi r_{SV,i}^2 + n_{LV,i} L_{LV,i} \pi r_{LV,i}^2}_{\substack{\text{Venous} \\ \text{contribution}}}} \tag{12}$$

where index i represents all vessel pathways (i.e., 171 pathways as described in 2.2.1; thus, index i ranges from 1 to 171), $n_{j,i}$ represents the number of vessels in compartment j along pathway i, $L_{j,i}$ represents the length of vessels in compartment j along pathway i, VOL_A is the total

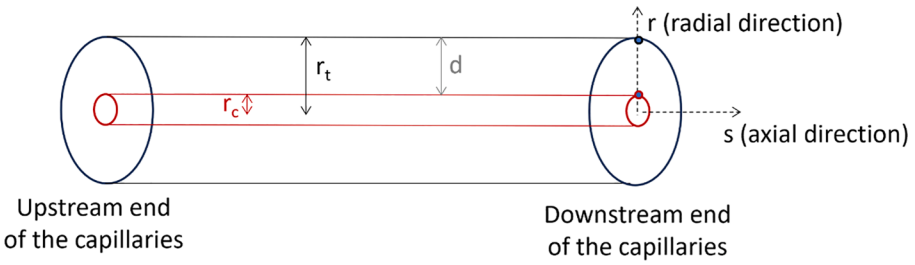

Fig. 3. Schematic of a single Krogh tissue cylinder. A sample capillary (red outline) is surrounded by a sleeve of tissue (black outline). The schematic depicts the radius of the capillary (r_c), the radius of the surrounding tissue (r_t), and the width of the surrounding tissue (d, gray). The red and black dot represent the starting and ending point of the curves depicted in Fig. 7 for PO_2 measures in tissue at the downstream end of the capillaries.

volume of the arteriolar network vessels and tissue (0.00115 cm^3), and the summation in the denominator represents the total volume of the downstream vessels and tissue (i.e., volume of the C, SV, and LV compartments). For an assumed vessel density, the tissue width (d) is calculated using Eq. (12). In the reference case of $VD = 500$ mm^{-2} [39], the tissue width d surrounding each capillary is 22 μm. Table 3 gives the range of computed values of d for simulated capillary densities between $VD = 250$ mm^{-2} and 750 mm^{-2}.

2.2.4. Vessel density simulations

The model is simulated for vessel density values ranging from 250 to 750 mm^{-2}. It is important to note that the common clinical definition of decreased VD referring to a reduction of the number of capillaries in a given area is qualitatively equivalent to the methodology conducted in the present study. Namely, decreased VD is achieved by increasing the radius of the Krogh tissue cylinder, which means that any given capillary is supplying oxygen to a larger tissue region, which is qualitatively equivalent to a region of tissue with fewer capillaries supplying it.

In each model simulation, the oxygen extraction fraction (OEF) is calculated as the ratio of oxygen consumption to oxygen delivery [40]:

$$OEF = \frac{\sum_{i=1}^{m} Q_i \cdot (SaO_2 - SvO_{2,i})}{Q_{total} \cdot SaO_2} \tag{13}$$

where m is the number of terminal arterioles (and thus downstream pathways), Q_i is the blood flow through the ith pathway, Q_{total} is the total blood flow through the full network, SaO_2 is the incoming arteriolar oxygen saturation to the network (assumed here to be 0.92 [41,42]), and $SvO_{2,i}$ is the outflow oxygen saturation at the downstream end of the ith capillary compartment.

In addition to OEF, oxygen saturation and/or PO_2 levels are predicted throughout the entire microvascular network and surrounding tissue as VD is varied for a range of oxygen demand ($M_0 = 1 - 4$ cm^3 O_2/100 cm^3/min). Additionally, simulations are conducted under conditions in which flow regulation mechanisms are not functional as a way to predict the impact of simultaneous vascular impairments that are characteristic of glaucoma. All simulations are run using C code, and the Green's function method is run using parallel processing to speed up computation time.

3. Results

3.1. Vessel densities obtained from clinical observations

Clinical data come from our ongoing prospective cross-sectional study of pre-perimetric open angle glaucoma patients ($n = 95$) and healthy controls free from eye disease ($n = 111$). One eye was randomly selected per subject for examination. Pre-perimetric open angle patients were under treatment with IOP-lowering medications, and their mean IOP was 16.1 (standard deviation: 4.7) mmHg. Further details regarding the clinical data are available here [10]. In these published clinical observations [10], pre-perimetric glaucoma patients demonstrated a 10–13 % reduction in VD compared to healthy, non-glaucomatous individuals. Specifically, computations of percentage area occupied by OCTA-detected vasculature revealed that whole image small vessel (SV) VD and global peripapillary SV VD were significantly lower in pre-perimetric OAG patients versus controls (43.99 (4.49) vs. 49.3 (2.5); $p < 0.001$, 10.8 % reduction) and (45.69 (6.02) vs. 51.89 (3.10); $p < 0.001$, reduction of 11.95 %). Whole image ALL VD and global peripapillary ALL VD were also both significantly lower in pre-perimetric OAG patients versus controls (49.62 (4.55) vs 55.55 (2.73); $p < 0.001$, reduction of 10.68 %) and (50.47 (8.07) vs 57.88 (3.20); $p < 0.001$, reduction of 12.81 %). Vessel densities were significantly lower for glaucoma patients than healthy individuals in all four quadrants ($p < 0.001$). Fig. 4 shows the means of measured vessel densities in the four quadrants, separated by glaucoma status (glaucoma/healthy).

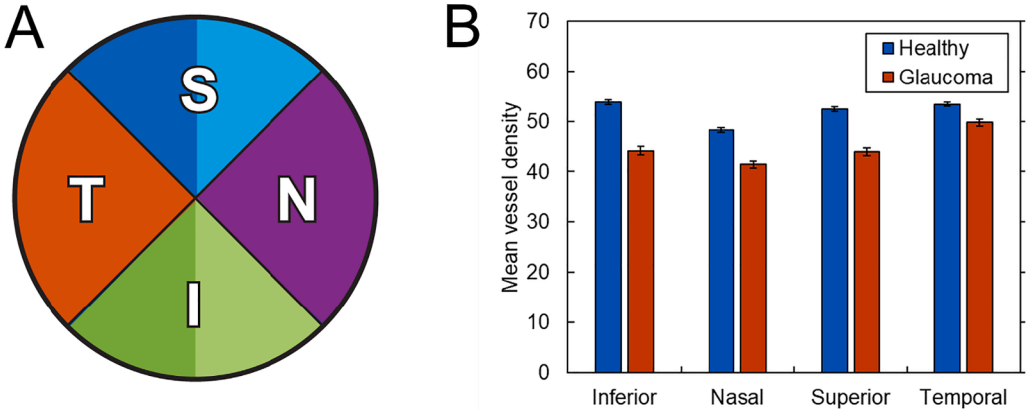

Fig. 4. A. Locations of superior (S), nasal (N), inferior (I), and temporal (T) quadrants in the eye. B. Measured vessel densities for healthy (blue) and glaucomatous (red) individuals in the four ocular quadrants. Mean ± SE. $N = 111$ healthy, $N = 95$ glaucoma [10].

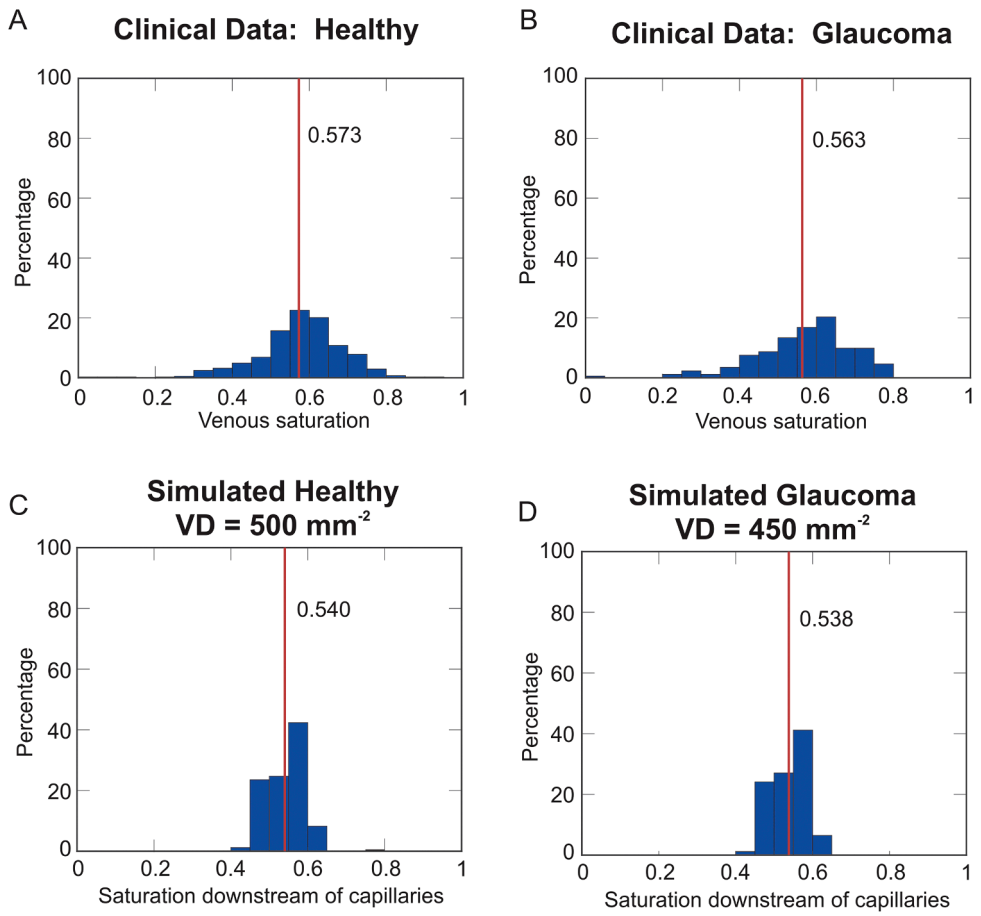

Fig. 5. Measured and simulated venous saturation. Clinically-measured venous saturation values obtained from retinal oximetry images in healthy (panel A) and early glaucoma patients (panel B). No error bars are shown, since this is a histogram showing the distribution of the full data set (with the average measured saturation indicated by the vertical red line). Venous blood oxygen saturation (i.e., at the downstream end of the capillaries) predicted using the mathematical model at baseline VD (i.e., simulated healthy VD = 500 mm^{-2}, panel C) and a 10 % decrease in VD (i.e., simulated early glaucoma VD = 450 mm^{-2}, panel D). Vertical red line in panels C and D denote the model-predicted average saturation across all pathways.

Measurements indicate a variation in vessel density by spatial region, both between glaucoma status groups and within.

3.2. Model validation

To validate model predictions, venous saturation values that were clinically measured from retinal oximetry in healthy and early glaucoma patients (histograms of the full distribution of patient saturation measurements are shown in Fig. 5A and 5B, respectively) are compared with mathematical model simulations at baseline VD (i.e., simulated healthy) and a 10 % decrease in VD (i.e., simulated early glaucoma) in Fig. 5C and 5D, respectively. There is a larger spread in clinically measured saturation values, but both measured and simulated data show a minor decrease in mean venous saturation (1.75 % and 0.4 %, respectively) values. This data set was not used to fit any model parameters. The alignment of model-predicted venous saturation levels with clinically-measured values validates the utility and accuracy of the mathematical model.

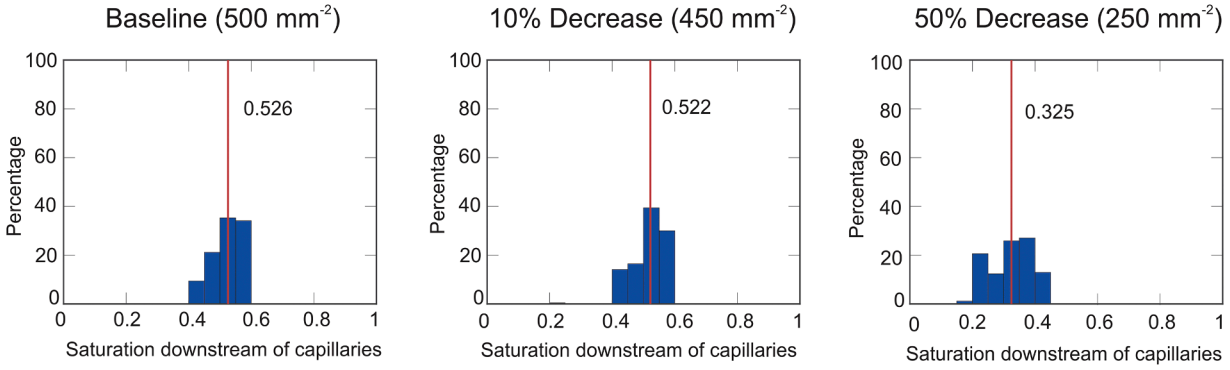

Fig. 6. Model predictions of oxyhemoglobin saturation of blood at the downstream end of the capillaries emanating from each of the terminal arterioles in the simulated network, for three values of vessel density: 500 mm^{-2} (left), 450 mm^{-2} (middle), and 250 mm^{-2} (right). The vertical red line indicates the average saturation across all pathways.

3.3. Model predicted impact of vessel density on retinal oxygenation

The theoretical model described in this study is used to assess the impact of these clinically observed changes in VD on oxygenation of retinal tissue and vessels. Larger changes observed in more advanced glaucoma cases [43] are also simulated with the model. Since a Krogh cylinder model is used to model oxygen diffusion in the capillaries, altering the overall density of capillaries translates into different Krogh tissue cylinder radii. For example, if VD is decreased, the radius of the Krogh tissue cylinder is increased (see Table 2).

Fig. 6 provides a histogram for the blood oxyhemoglobin saturation calculated immediately downstream of the capillaries assuming an oxygen demand of M_0 = 2 cm^3 O_2/100 cm^3/min and fully functional regulation mechanisms. The model predicts a 1 % and 38 % decrease in mean saturation (mean values are denoted by vertical red lines) in retinal vessels immediately downstream of the capillaries when VD is decreased from its reference value of 500 mm^{-2} by 10 % and 50 %, respectively, indicating that for smaller (10 %) decreases in VD, blood flow regulation mechanisms provide compensation to maintain oxygen saturation levels near baseline. Additionally, a greater spread in PO_2 values is predicted at lower values of VD.

The mean values of the oxyhemoglobin saturation downstream of the capillaries are shown for a wider range of VD values in Fig. 7A. The model is also used to predict the impact of vessel density on oxygen extraction fraction (Fig. 7B). As expected, the decrease in oxygen saturation with decreased vessel density corresponds to an increase in the oxygen extraction fraction. In both panels, model predictions are given for three levels of oxygen demand: M_0 = 1 (low, blue), 2 (moderate, red) and 4 (high, black) cm^3 O_2/100 cm^3/min with all flow regulation mechanisms functional. For the lowest VD value considered (250 mm^{-2}), the oxygen extraction fraction is maximal (at 1, or 100 %) for M_0 = 4 cm^3 O_2/100 cm^3/min. For M_0 = 1 cm^3 O_2/100 cm^3/min, saturation does not change much over the entire range of simulated VD values. However, the vascular smooth muscle tone (activation) varies between 0 and 1, suggesting that the ability to regulate flow allows the vasculature to compensate for reduced VD levels. However, as oxygen demand is increased, the vasculature reaches its maximum regulatory capacity, and thus impairments in oxygenation are observed via the decreases in venous saturation.

The impact of decreased VD on downstream tissue oxygenation is shown in Fig. 8 for an oxygen demand of M_0 = 2 cm^3 O_2/100 cm^3/min. The mean tissue PO_2 calculated for all Krogh tissue cylinders is depicted as a function of radial position, and five different values of VD are depicted: 750 mm^{-2} (magenta), 550 mm^{-2} (cyan), 500 mm^{-2} (black), 450 mm^{-2} (red), and 250 mm^{-2} (blue). Thus, all curves begin at 3 μm, corresponding to the radius of the capillaries (r_c), and extend to the radius of the Krogh tissue cylinder (r_t), which ranges from about 20–36 μm based on tissue widths for each VD value (as depicted in Fig. 3). As expected, as VD is decreased, PO_2 also decreases at r_c = 3 μm. Interestingly, there are even larger decreases in PO_2 into the tissue (i.e., in the radial direction) at smaller VD values. The mean tissue PO_2 near zero for a VD of 250 mm^{-2} indicates that several pathways are hypoxic (PO_2 = 0 mmHg) under those conditions.

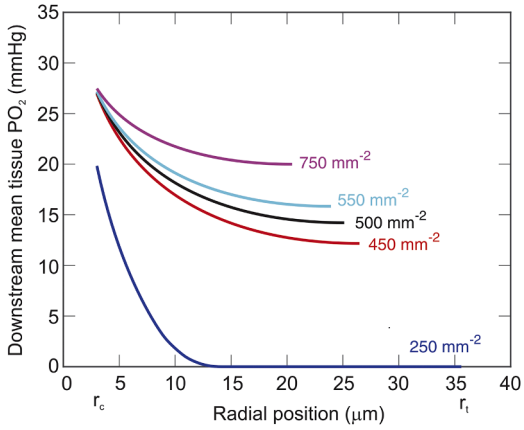

Fig. 8. Tissue PO_2 at the downstream end of the capillaries as a function of tissue radius (radial position) for five values of vessel density: 750 mm^{-2} (magenta), 550 mm^{-2} (cyan), 500 mm^{-2} (black), 450 mm^{-2} (red), and 250 mm^{-2} (blue). The positions at which these predictions are obtained are shown in Fig. 3. Model simulations are conducted for an oxygen demand of M_0 = 2 cm^3 O_2/100 cm^3/min with all flow regulation mechanisms functional.

Since glaucoma is characterized by multiple vascular impairments in addition to capillary loss, the model is used to simulate the impact of capillary loss in combination with impaired flow regulation mechanisms on retinal oxygenation and flow in Fig. 9 for an oxygen demand of M_0 = 2 cm^3 O_2/100 cm^3/min. Impaired flow regulation is simulated in the model by keeping the components of S_{tone} (Eq. (3)) at their control state values to prevent a change in vessel diameter in response to changing pressure, shear stress, or oxygen level. When flow regulation is functional, a large change in flow is possible over the range of simulated VD

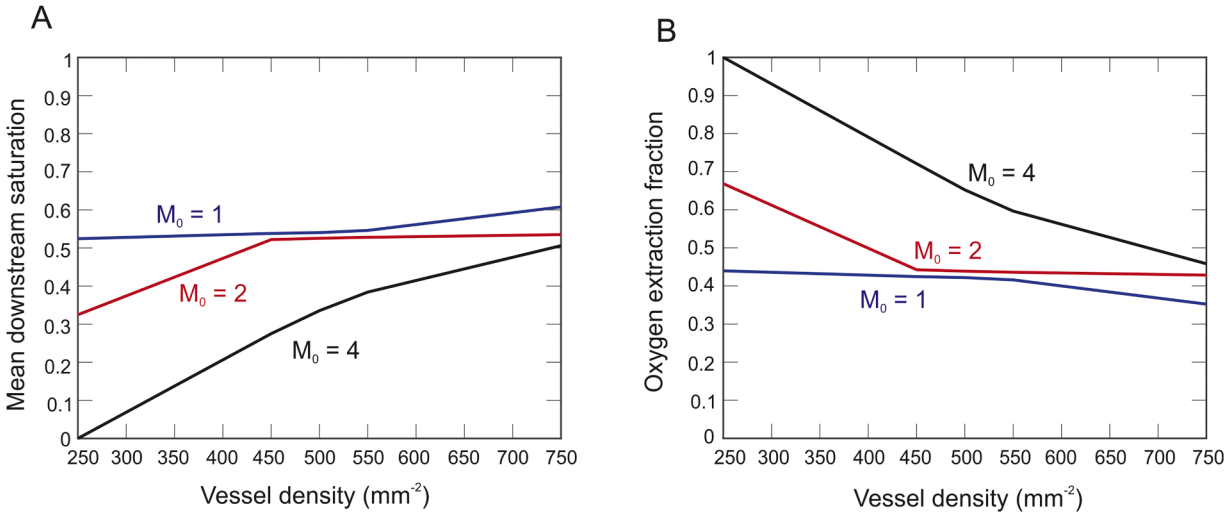

Fig. 7. A. Oxyhemoglobin saturation of blood at the downstream end of the capillaries as vessel density is varied among five values: 250 mm^{-2}, 450 mm^{-2}, 500 mm^{-2}, 550 mm^{-2}, and 750 mm^{-2}. B. The oxygen extraction fraction (OEF) is shown as a function of vessel density. Model simulations are conducted for a low (M_0 =1 cm^3 O_2/100 cm^3/min, blue), moderate (M_0 =2 cm^3 O_2/100 cm^3/min, red), and high (M_0 = 4 cm^3 O_2/100 cm^3/min, black) level of oxygen demand.

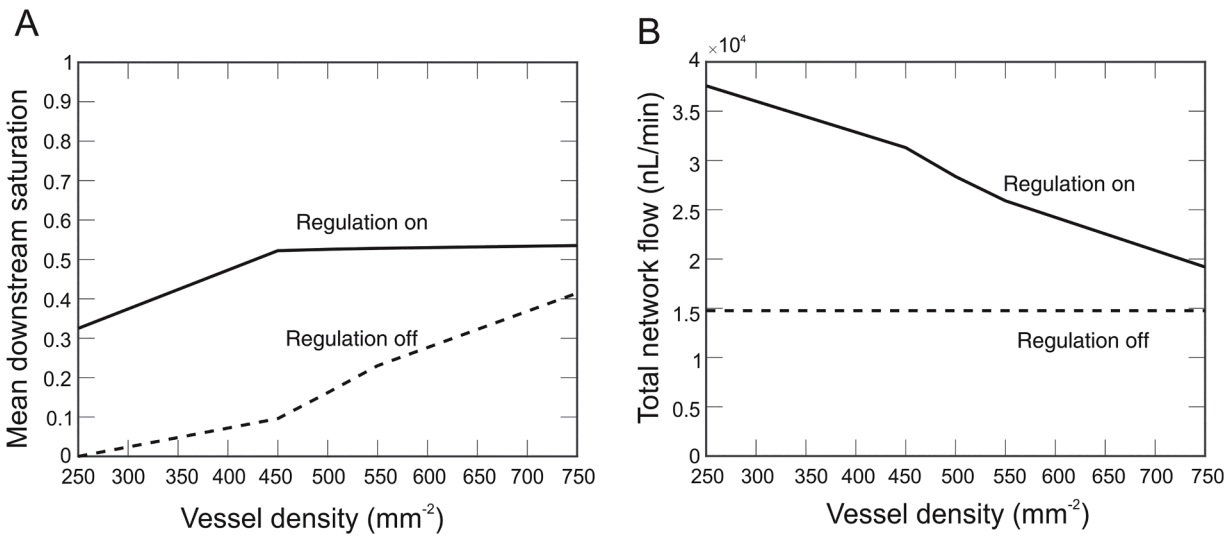

Fig. 9. Oxyhemoglobin saturation of blood at the downstream end of the capillaries (panel A) and total network flow (panel B) as vessel density is varied from 250 mm^{-2} to 750 mm^{-2}. Simulations are provided in the presence (solid) and absence (dashed) of flow regulation mechanisms.

values (Fig. 9B), which translates to relatively constant saturation levels until VD is decreased dramatically (Fig. 9A). However, when flow regulation is impaired, a dramatic impact on oxygen saturation is predicted. At a baseline level of VD = 500 mm^{-2}, impairing regulation leads to a 69 % decrease in saturation while a 50 % decrease in vessel density leads to a 38 % decrease in saturation. If both regulation is impaired and vessel density is decreased by 50 %, saturation is predicted to decrease by 100 %. A similar result of near-zero saturation was also predicted for just a 10 % decrease in VD if, in addition to impaired regulation, oxygen demand (M_0) was doubled to 4 cm^3 O_2/100 cm^3/min (not shown), indicating that a combination of high oxygen demand and impaired regulation can lead to large decreases in oxygenation even for small decreases in vessel density.

4. Discussion

4.1. Clinical perspectives from theoretical predictions

This study uses a theoretical model to predict the impact of clinical measures of VD on the retinal circulation and tissue oxygenation. Understanding the consequences of hemodynamic and metabolic disturbances helps to reveal the mechanisms involved in eye disease. Specifically, impaired vascular factors have been long associated with glaucomatous disease, with pilot data linking impaired blood flow to biomarkers of disease progression [1]. Recently, we reported significant early reductions in the VD of the peripapillary retina, ONH, and macular regions in pre-perimetric glaucoma patients compared to healthy controls [10]. Herein, we use a validated [16] theoretical model to describe the impact of reduced VD on retinal perfusion and oxygen metabolism.

Our clinical observations demonstrate a moderate, yet significant (10–13 %), reduction in VD in pre-perimetric glaucoma patients. Following a reduction in VD by 10 %, the theoretical model predicted a corresponding decrease in retinal tissue oxygenation. This suggests that observed decreases in VD may be a precursor to larger blood flow and oxygenation impairments in more advanced stages of glaucoma, possibly initiating a negative feedback loop that goes undetected in early glaucoma diagnostics, including visual fields.

The theoretical model results showed a nonlinear relationship between the decrease in VD and the effect on downstream saturation, indicating that larger decreases in VD have a disproportionate impact on oxygenation. The model results also indicated that the detrimental effects of minor reductions in VD are exacerbated when combined with other vascular impairments. For example, an increase in oxygen demand (i.e., M_0) combined with a decrease in VD was shown to yield abnormal oxygenation and areas of hypoxia. Similarly, impaired flow regulation mechanisms combined with decreased VD and/or increased M_0 led to very significant reductions in oxygen saturation (Fig. 9A). These predictions suggest that while an otherwise healthy patient may be able to compensate for reduced VD (to some extent), decreased VD combined with other vascular impairments could trigger a constellation of negative consequences that result in glaucoma. This study provides convincing evidence of potential effects of reduced VD on tissue oxygenation that are not currently observed in the clinic via oximetry and suggests that reductions in vessel density may represent a precursor to visual field loss.

Blood flow regulation mechanisms are predicted to be able to dampen the effects of a small reduction in VD (Fig. 6, middle), but as the VD reduction grows, regulation cannot prevent further decreases in oxygenation (Fig. 6, right). At a low oxygen demand level, a 50 % decrease in VD led to only a 3 % decrease in mean downstream oxygen saturation. Maintaining the oxygen saturation was accomplished via an 86 % decrease in smooth muscle activation (i.e., significant vasodilation). However, at a moderate oxygen demand level, vessels were already nearly fully dilated, and thus a 50 % decrease in VD led to a 38 % decrease in oxygen saturation. The clinical implication is that detecting VD changes early – before other indicators of glaucoma become observable – can potentially prevent more significant decreases in VD (or other vascular impairments) typically seen in advanced stages of glaucoma.

4.2. Limitations

As with any theoretical model, assumptions are made that lead to some model limitations. For example, the current network geometry accounts only for heterogeneity in the arteriolar network structure, although the assignment of fractional flows to capillary compartments helps to maintain the impact of the spatial heterogeneity of the arteriolar network. The use of compartments for capillaries, small venules, and large venules could be altered in the future to introduce a capillary mesh in different retinal layers and a heterogeneous network structure for venules. Such an adaptation would cause significant increases in computational time and is not predicted to alter tissue oxygenation predictions substantially. The numbers of capillaries, small venules, and large venules in the current compartmental version of the downstream microcirculation were dictated by the conservation of flow. However, different assumptions regarding symmetry of vessels could be simulated

to assess the impact of varying the proportion of C, SV, and LV vessels downstream of each terminal arteriole.

The network structure is physiological since it originates from a mouse vascular network, but it did not originate from a human retinal vasculature image. Future work will involve the digitization of images obtained from retinal oximetry or fundus photography to generate predictions that are patient-specific or at least averaged over numerous healthy patients and glaucomatous patients. Future work also aims to include multiple parallel compartments to represent capillaries in the superficial, intermediate, and deep plexuses, since capillary densities differ in each plexus. Also, the current model conserves vessel volume in the system; future work could consider implementation of the Krogh cylinder model in which total vessel plus tissue volume is conserved. Additionally, while elevated intraocular pressure is a key risk factor for glaucoma, IOP is not varied in this study in an effort to isolate the impact of VD on tissue oxygenation. However, the impact of IOP as well as varying mean arterial pressure will be examined in a separate study, and future work will also account for venous collapsibility.

4.3. Summary

Ultimately, the mathematical model utilized in this study demonstrated the significant detrimental impact of a reduced vascular density on the oxygenation of retinal tissues. Quantifying the impact of decreased VD on oxygenation of the retina provides a translatable framework for improving predictive risk modeling in glaucoma. Future research should seek to test predictability of modeling outputs with clinical observations of disease progression over time.

Funding

JA gratefully acknowledges NSF DMS-1,654,019 and NSF DMS-2,150,108. JA, BF, AH, BS, and AV gratefully acknowledge NIH R01EY030851. AH is supported by NIH grants (R01EY030851 and R01EY034718), NYEE Foundation grants, and in part by a Challenge Grant award from Research to Prevent Blindness, NY.

CRediT authorship contribution statement

Brendan C. Fry: Writing – review & editing, Writing – original draft, Validation, Supervision, Project administration, Methodology, Funding acquisition, Formal analysis, Data curation, Conceptualization. **Croix Gyurek:** Visualization, Methodology, Investigation, Data curation. **Amanda Albright:** Visualization, Methodology, Data curation. **George Eckert:** Writing – review & editing, Writing – original draft, Validation, Formal analysis, Data curation. **Janet Coleman-Belin:** Writing – original draft, Data curation. **Alice Verticchio:** Investigation, Funding acquisition, Formal analysis, Data curation, Conceptualization. **Brent Siesky:** Writing – review & editing, Writing – original draft, Supervision, Investigation, Funding acquisition, Formal analysis, Data curation, Conceptualization. **Alon Harris:** Writing – review & editing, Writing – original draft, Supervision, Project administration, Methodology, Investigation, Funding acquisition, Formal analysis, Data curation, Conceptualization. **Julia Arciero:** Writing – review & editing, Writing – original draft, Visualization, Validation, Supervision, Project administration, Methodology, Investigation, Funding acquisition, Formal analysis, Data curation, Conceptualization.

Declaration of competing interest

There are no conflicts of interest. Professor Alon Harris would like to disclose that he received remuneration from AdOM, Qlaris, and Cipla for serving as a consultant, and he serves on the board of AdOM, Qlaris and SlitLed. Professor Alon Harris holds an ownership interest in AdOM, Oxymap, Qlaris, and SlitLed. If you have questions regarding paid relationships that your physician/researcher may have with industry, you are encouraged to talk with your physician/researcher, or check for industry relationships posted on individual faculty pages on our website at http://icahn.mssm.edu/.

Data availability

Data will be made available on request.

Acknowledgements

Some of the methods and results of this paper were presented at the ARVO Annual Meeting 2023.

References

[1] A. Harris, et al., Ocular blood flow as a clinical observation: value, limitations and data analysis, Prog. Retin. Eye Res. (2020) 100841.
[2] H. Akil, et al., Retinal vessel density from optical coherence tomography angiography to differentiate early glaucoma, pre-perimetric glaucoma and normal eyes, PLoS One 12 (2) (2017) e0170476.
[3] H.S. Chen, et al., Optical Coherence Tomography Angiography of the Superficial Microvasculature in the Macular and Peripapillary Areas in Glaucomatous and Healthy Eyes, Invest. Ophthalmol. Vis. Sci. 58 (9) (2017) 3637–3645.
[4] T. Mansoori, et al., Radial peripapillary capillary density measurement using optical coherence tomography angiography in early glaucoma, J. Glaucoma 26 (5) (2017) 438–443.
[5] G. Triolo, et al., Optical coherence tomography angiography macular and peripapillary vessel perfusion density in healthy subjects, glaucoma suspects, and glaucoma patients, Invest. Ophthalmol. Vis. Sci. 58 (13) (2017) 5713–5722.
[6] A. Yarmohammadi, et al., Relationship between optical coherence tomography angiography vessel density and severity of visual field loss in glaucoma, Ophthalmology 123 (12) (2016) 2498–2508.
[7] A. Yarmohammadi, et al., Optical coherence tomography angiography vessel density in healthy, glaucoma suspect, and glaucoma eyes, Invest. Ophthalmol. Vis. Sci. 57 (9) (2016) OCT451–OCT459.
[8] J.D. Shin, et al., Vascular biomarkers from optical coherence tomography angiography and glaucoma: where do we stand in 2021? Acta Ophthalmol 100 (2) (2022) e377–e385.
[9] A.I.M. Miguel, A.B. Silva, L.F. Azevedo, Diagnostic performance of optical coherence tomography angiography in glaucoma: a systematic review and meta-analysis, Br. J. Ophthalmol. 103 (11) (2019) 1677–1684.
[10] A. Verticchio Vercellin, et al., Regional vessel density reduction in the macula and optic nerve head of patients with pre-perimetric primary open angle glaucoma, J. Glaucoma 32 (11) (2023) 930–941.
[11] B.C. Fry, T.K. Roy, T.W. Secomb, Capillary recruitment in a theoretical model for blood flow regulation in heterogeneous microvessel networks, Physiol. Rep. 1 (3) (2013) e00050.
[12] D. Goldman, R.M. Bateman, C.G. Ellis, Effect of sepsis on skeletal muscle oxygen consumption and tissue oxygenation: interpreting capillary oxygen transport data using a mathematical model, Am. J. Physiol. Heart Circ. Physiol. 287 (6) (2004) H2535–H2544.
[13] T.W. Secomb, et al., Theoretical simulation of oxygen transport to brain by networks of microvessels: effects of oxygen supply and demand on tissue hypoxia, Microcirculation 7 (4) (2000) 237–247.
[14] G. Chiaravalli, et al., A multi-scale/multi-physics model for the theoretical study of the vascular configuration of retinal capillary plexuses based on OCTA data, Math. Med. Biol. 39 (1) (2022) 77–104.
[15] J.P. Campbell, et al., Detailed vascular anatomy of the human retina by projection-resolved optical coherence tomography angiography, Sci. Rep. 7 (2017) 42201.
[16] A. Albright, et al., Metabolic blood flow regulation in a hybrid model of the human retinal microcirculation, Math. Biosci. 357 (2023) 108969.
[17] J. Arciero, et al., Metabolic signaling in a theoretical model of the human retinal microcirculation, Photonics 8 (10) (2021).
[18] H.L. Rao, et al., Optical coherence tomography angiography in glaucoma, J. Glaucoma 29 (4) (2020) 312–321.
[19] A.H. Kashani, et al., Optical coherence tomography angiography: a comprehensive review of current methods and clinical applications, Prog. Retin. Eye Res. 60 (2017) 66–100.
[20] A. Koustenis Jr., et al., Optical coherence tomography angiography: an overview of the technology and an assessment of applications for clinical research, Br. J. Ophthalmol. 101 (1) (2017) 16–20.
[21] R.X.A. System (Ed.), RTVue XR Avanti User Manual, Optovue, Inc., Fremond, CA, USA, 2014. Editor.
[22] D. Prada, et al., Autoregulation and neurovascular coupling in the optic nerve head, Surv. Ophthalmol. 61 (2) (2016) 164–186.
[23] RTVue XR Avanti User Manual, Optovue, Inc, 2019.
[24] L. Carichino, Y. Arieli G.G., B.A. Siesky, A. Harris, Effect of lamina cribrosa deformation on hemodnamics of the central retinal artery: a mathematical model, in: ARVO Annual Meeting, 2012.

[25] D.M. Young, Iterative methods for solving partial difference equations of elliptic type, Trans. Am. Math. Soc. 76 (1954) 92–111.
[26] J.C. Arciero, B.E. Carlson, T.W. Secomb, Theoretical model of metabolic blood flow regulation: roles of ATP release by red blood cells and conducted responses, Am. J. Physiol. Heart Circ. Physiol. 295 (4) (2008) H1562–H1571.
[27] B.E. Carlson, J.C. Arciero, T.W. Secomb, Theoretical model of blood flow autoregulation: roles of myogenic, shear-dependent, and metabolic responses, Am. J. Physiol. Heart Circ. Physiol. 295 (4) (2008) H1572–H1579.
[28] J. Arciero, et al., Theoretical analysis of vascular regulatory mechanisms contributing to retinal blood flow autoregulation, Invest. Ophthalmol. Vis. Sci. 54 (8) (2013) 5584–5593.
[29] B.C. Fry, et al., Blood flow regulation and oxygen transport in a heterogeneous model of the mouse retina, Math. Biosci. 329 (2020) 108476.
[30] B.E. Carlson, T.W. Secomb, A theoretical model for the myogenic response based on the length-tension characteristics of vascular smooth muscle, Microcirculation 12 (4) (2005) 327–338.
[31] M.L. Ellsworth, A.S. Popel, R.N. Pittman, Assessment and impact of heterogeneities of convective oxygen transport parameters in capillaries of striated muscle: experimental and theoretical, Microvasc. Res. 35 (3) (1988) 341–362.
[32] T.B. Bentley, H. Meng, R.N. Pittman, Temperature dependence of oxygen diffusion and consumption in mammalian striated muscle, Am. J. Physiol. 264 (6 Pt 2) (1993) H1825–H1830.
[33] A.S. Golub, R.N. Pittman, Oxygen dependence of respiration in rat spinotrapezius muscle in situ, Am. J. Physiol. Heart Circ. Physiol. 303 (1) (2012) H47–H56.
[34] R. Hsu, T.W. Secomb, A Green's function method for analysis of oxygen delivery to tissue by microvascular networks, Math. Biosci. 96 (1) (1989) 61–78.
[35] T.W. Secomb, A Green's function method for simulation of time-dependent solute transport and reaction in realistic microvascular geometries, Math. Med. Biol. 33 (4) (2016) 475–494.
[36] A.S. Popel, Theory of oxygen transport to tissue, Crit. Rev. Biomed. Eng. 17 (3) (1989) 257–321.
[37] A. Krogh, The number and distribution of capillaries in muscles with calculations of the oxygen pressure head necessary for supplying the tissue, J. Physiol. 52 (6) (1919) 409–415.
[38] L. Carichino, et al., A theoretical investigation of the increase in venous oxygen saturation levels in glaucoma patients, Invest. Ophthalmol. Vis. Sci. 56 (7) (2015).
[39] B.J. McGuire, T.W. Secomb, Estimation of capillary density in human skeletal muscle based on maximal oxygen consumption rates, Am. J. Physiol. Heart Circ. Physiol. 285 (6) (2003) H2382–H2391.
[40] A.E. Felder, et al., Inner retinal oxygen extraction fraction in response to light flicker stimulation in humans, Invest. Ophthalmol. Vis. Sci. 56 (11) (2015) 6633–6637.
[41] A. Geirsdottir, et al., Retinal vessel oxygen saturation in healthy individuals, Invest. Ophthalmol. Vis. Sci. 53 (9) (2012) 5433–5442.
[42] F.C. Delori, Noninvasive technique for oximetry of blood in retinal vessels, Appl. Opt. 27 (6) (1988) 1113–1125.
[43] S. Sefic, et al., Assessment of perfused peripapillary capillaries and peripapillary capillary density maps in glaucoma patients, Med. Arch. 74 (4) (2020) 275–278.